Neurosci. Bull.
https://doi.org/10.1007/s12264-025-01497-y

www.neurosci.cn
www.springer.com/12264

ORIGINAL ARTICLE

Deletion of the SHORT Syndrome Gene *Prkce* Results in Brain Atrophy and Cognitive and Motor Behavior Deficits in Mice

Yu-Long Bao[1] · Wei-Peng Duan[1] · Yan Yang[1,2] · Zhijie Lin[1] · Ying Shen[3,4] · Rui Zheng[2] · Xin-Tai Wang[1]

Received: 31 March 2025 / Accepted: 22 May 2025

Abstract The neurological manifestations of SHORT syndrome include intrauterine growth restriction, microcephaly, intellectual disability, hearing loss, and speech delay. SHORT syndrome is generally believed to be caused by *PIK3R1* gene mutations and impaired PI3K-AKT activation. Recently, a clinical case report described a SHORT syndrome with a novel mutant in *PRKCE* gene encoding protein kinase Cε (PKCε). However, it remains unclear whether the down-regulation of PKCε gives rise to the symptoms of SHORT syndrome. In this study, we show that a deficiency of PKCε in the central nervous system leads to cerebral and cerebellar atrophy, as well as motor and social deficits. Mechanistically, the deletion of PKCε results in the down-regulation of VEGF/PI3K-induced AKT activation, thereby causing abnormal brain development and dysfunctions. These findings emphasize the roles of PKCε in the development and function of the brain, and offer new perspectives for understanding the neurological manifestations of SHORT syndrome.

Keywords PKCε · AKT · SHORT syndrome · Cognition · Motor

Introduction

SHORT (short stature, hyperextensibility, ocular depression, Rieger anomaly, and teething delay) is a rare malformation syndrome, with ~50 confirmed case reports. The most common features of SHORT syndrome include intrauterine growth restriction, postnatal growth restriction, lipoatrophy, and facial gestalt [1, 2]. With the progress of clinical diagnosis, microcephaly and significant intellectual disability have also been unequivocally identified as part of the SHORT syndrome phenotype [3–5]. Therefore, the neurodevelopmental and functional impairments in SHORT syndrome merit more attention.

It has been established that the pathological mechanism underlying SHORT syndrome is closely associated with mutations in phosphoinositide-3-kinase regulatory subunit

Yu-Long Bao and Wei-Peng Duan contributed equally to this work.

Supplementary Information The online version contains supplementary material available at https://doi.org/10.1007/s12264-025-01497-y.

✉ Ying Shen
yshen@zju.edu.cn

✉ Rui Zheng
zhengr@zju.edu.cn

✉ Xin-Tai Wang
xintaiouc@163.com

1 Zhejiang Key Laboratory of Organ Development and Regeneration, College of Life and Environmental Sciences, Hangzhou Normal University, Hangzhou 311121, China

2 The Children's Hospital, National Clinical Research Center for Child Health, Zhejiang University School of Medicine, Hangzhou 310052, China

3 Department of Physiology and Center for Brain Health of the Fourth Affiliated Hospital, Zhejiang University School of Medicine, Hangzhou 310058, China

4 Department of Neurology, Institute of Neuroscience, Key Laboratory of Neurogenetics and Channelopathies of Guangdong Province and the Ministry of Education of China, The Second Affiliated Hospital, Guangzhou Medical University, Guangzhou 510260, China

1 (*PIK3R1)* [4, 6–10], which encodes the regulatory subunit (p85α) of phosphatidylinositol 3-kinase (PI3K). PI3K catalyzes the conversion of phosphatidylinositol 4,5-bisphosphate (PIP2) to phosphatidylinositol 3,4,5-trisphosphate (PIP3), thereby activating protein kinase B (PKB, also known as AKT) [11]. Notably, *PIK3R1* mutations linked to SHORT syndrome predominantly occur within the C-terminal Src homology 2 (SH2) domain, disrupting the interaction between the regulatory and catalytic subunits of PI3K and consequently reducing PI3K activity [4]. The *PIK3R1* mutation influences pathophysiological processes such as cell proliferation, differentiation, apoptosis, and migration by modulating the AKT activity [12–14].

Mutations in the *Prkce* gene, responsible for encoding PKCε (protein kinase Cε), have emerged as key causative factors in a diverse range of diseases. This includes malignancies [15], insulin resistance [16], type 2 diabetes [17], and various neurological disorders. The latter category specifically covers Alzheimer's disease [18–20], neuropathic pain [21], and alcohol use disorders [22]. Recently, Alcantara *et al*. identified *PRKCE* as the second pathogenic gene associated with SHORT syndrome. Their research demonstrated that a heterozygous mutation (E599K) in PKCε leads to functional loss of PKCε [14]. However, the precise pathological mechanisms underpinning the connection between PKCε mutations and the symptoms of SHORT syndrome remain unclear and require further investigation.

In this study, we created a conditional knockout mouse model with PKCε deficiency specifically in the central nervous system to systematically evaluate its influence on neurodevelopment and behavior. Our results clearly show that hippocampal and cerebellar development is severely impaired in these conditional knockout mice. These developmental defects are closely associated with deficits in multiple functional domains, including working memory, social novelty preference, and motor coordination. In contrast, conditional deletion of PKCε in GABAergic neurons had no discernible effect on brain development. In addition, we demonstrated that ablation or pharmacological inhibition of PKCε activity led to a significant reduction in VEGF/PI3K-mediated AKT activation. These findings suggest that modulation of the VEGF/PI3K/AKT pathway is a potential molecular mechanism through which PKCε regulates hippocampal and cerebellar development, as well as cognitive and motor functions.

Materials and Methods

Animals

Mice were bred in the Experimental Animal Center of Hangzhou Normal University under a 12:12 h dark/light cycle. *PKCε*$^{F/F}$ mice were generated with the assistance of GemPharmatech (Jiangsu, China). *VGAT*^{Cre} mice were obtained from Yanmei Tao (Southeast University, Nanjing, China). Conditional knockout mice (*PKCε*$^{F/F}$;*Nestin*^{Cre} or *PKCε*$^{F/F}$;*VGAT*^{Cre}) were obtained by crossing control mice (*PKCε*$^{F/F}$) with *Nestin*^{Cre} or *VGAT*^{Cre} mice. The resulting offspring were genotyped using polymerase chain reaction (PCR) of genomic DNA, which were: *PKCε* floxP fragment, F (forward): 5'-TGG ACA ATC TTG GCA TCG GAT C-3'; R (reverse): 5'-GAT GGT TGT GAC TAG CAG AGA GG-3'; *Nestin*^{Cre}, F: 5'-TCG ATG CAA CGA GTG ATG AG-3'; R: 5'-TCC ATG AGT GAA CGA ACC TG -3'; *VGAT*^{Cre}, F: 5'-TGC CAG GAT CAG GGT TAA AG-3'; R: 5'-GCT TGC ATG ATC TCC GGT AT-3'. Male mice's age-matched littermates were selected at random for each experiment. All procedures were approved by the Animal Care and Use Committee of the Hangzhou Normal University and were performed according to the National Institutes of Health Guide for the Care and Use of Laboratory Animals.

Reverse Transcription (RT)-PCR

By using a patch-clamp pipette, the material from each Purkinje cell was extracted and transferred to a Qiagen One Step RT-PCR Kit (Cat# 210212, Qiagen, Maryland, USA). The primers were: *Gapdh* F: GGT GAA GGT CGG TGT GAA CG; *Gapdh* R: CTC GCT CCT GGA AGA TGG TG; *Prkce* F: ATG ACC AAG AAC CCG CA; *Prkce* R: CCA GCA GTA CCC AGT CAA TC.

Antibodies

Anti-GluA1 (Cat# 04-855, RRID:AB_1977216), GluA2 (Cat# MAB397, RRID:AB_2113875), vGluT1 (Cat# ABN1647, RRID:AB_2814811), NeuN (Cat# MAB377, RRID:AB_2298772), GAD67 (Cat# MAB5406, RRID:AB_2278725), and vGluT2 (Cat# MAB5504, RRID:AB_2187552) antibodies were from Millipore (Billerica, USA). Anti-PI3K (Cat# HA601206, RRID:AB_3071925) was from HuaBio (Hangzhou, China). Anti-PKCε (Cat# 20877-1-AP, RRID:AB_10697812) was from Proteintech (Rosemont, USA). Anti-PKCε-pSer729 (Cat# ab63387, RRID:AB_1142277) was from Abcam (Cambridge, UK). Anti-PSD95 (Cat# 3450, RRID:AB_2292883), AKT (Cat# 4691, RRID:AB_915783), AKT-pSer473 (Cat# 4060, RRID:AB_2315049), and AKT-pThr308 (Cat# 2965, RRID:AB_2255933) were from Cell Signaling Technology (Danvers, USA). Anti-calbindin (Cat# C9848, RRID:AB_476894) was from Sigma-Aldrich (St. Louis, USA). Anti-mGlu1 (Cat# 610965, RRID:AB_398278) was from BD Biosciences (Billerica, USA). Antibodies against β-tubulin (Cat# sc-5274, RRID:AB_2288090) and β-actin (Cat# sc-47778, RRID:AB_626632) were from Santa Cruz Biotechnology (Dallas, USA). Anti-vGluT1

(Cat# 135 304, RRID:AB_887878) was from Synaptic Systems (Göttingen, Germany). Anti-PKCε (Cat# MA5-14908, RRID:AB_10985232), horseradish peroxidase (HRP)-conjugated secondary antibodies, and Alexa Fluor-conjugated secondary antibodies were from Thermo (Waltham, USA).

Cell Culture and Drug Treatment

Neuro-2A (N2A) cells were cultured in Dulbecco's modified Eagle medium (DMEM, Cat# 11965092, Gibco, New York, USA) with 10% fetal bovine serum (FBS, Cat# 10100147C, Gibco, New York, USA). Cells were treated with the PKCε agonist DCP-LA (100 nmol/L, Cat# HY-108599, MCE, New Jersey, USA), or vascular endothelial growth factor (VEGF, 30 ng/mL, Cat# C744, Novoprotein, Suzhou, China), or the PKCε inhibitor ε-V1-2 (5 μmol/L, Cat# HY-P0154, MCE, New Jersey, USA) for 60 min. Cells were lysed in 1% Triton X-100 buffer with protease inhibitor, then centrifuged at 12,000 × *g* at 4°C for 30 min. The supernatant and pellet fractions were retained as Triton X-100-soluble (S) and Triton X-100-insoluble (In) fractions.

Co-Immunoprecipitation (Co-IP)

The cerebellum was lysed in radio immunoprecipitation assay (RIPA) buffer (in mmol/L: 50 Tris, 100 NaCl, 1 ethylenediaminetetraacetic acid (EDTA), 0.5% sodium deoxycholate, 0.2% sodium dodecyl sulfate (SDS), 1% Triton X-100, pH 7.4) and centrifuged at 16,000 × *g* for 10 min. The supernatant was supplemented with protein A-sepharose beads and rabbit anti-PKCε antibody (1:200). Following 3 washes in RIPA buffer, 2 × SDS sample buffer was used to extract the proteins from the beads.

Western Blot

The Western blots followed prior research [23]. The dilutions of antibodies were GluA1 (1:2,000), GluA2 (1:2,000), vGluT1 (1:2,000), vGluT2 (1:2,000), PI3K (1:1,000), PKCε (1:2,000), PKCε-pSer729 (1:1,000), PSD95 (1:5,000), AKT (1:2,000), AKT-pSer473 (1:1,000), AKT-pThr308 (1:1,000), mGlu1 (1:2,000), β-tubulin (1:5,000), β-actin (1:5,000), and HRP-conjugated secondary antibodies (1:10,000).

Immunofluorescence Staining

The immunohistochemical staining followed prior research [24]. The antibody dilutions were calbindin (1:500), PKCε (1:200), NeuN (1:500), GAD67 (1:500), vGluT1 (1:500), and Alexa Fluor-conjugated secondary antibodies (1:1,000). The images were acquired with a Zeiss LSM710 confocal microscope (Jena, Germany).

N2A cells were fixed in 4% paraformaldehyde, and cell membranes were permeabilized with 0.2% Triton X-100. After blocking with 10% bovine serum albumin (BSA), cells were incubated with primary antibodies and Alexa Fluor-conjugated secondary antibodies. The primary antibody dilutions were PKCε (1:500) and Alexa Fluor-conjugated secondary antibodies (1:1,000). Cells were incubated in phalloidin solution (C2201S, Beyotime, Shanghai, China) for 1 h, and sealed with proLong gold anti-fade reagents (Thermo, P36931).

PKCε membrane expression in cultured N2A cells was measured using ImageJ software (National Institutes of Health, Maryland, USA) with the MorphoLibJ plugin. Generally, fluorescence images were filtered by a Gaussian blur, and the red (phalloidin) channel was selected and used as a mask for the green (PKCε) channel, overlapping to automatically filter out the cell membrane PKCε. The mean gray value was calculated as fluorescence intensity.

Nissl Stain

The Nissl staining kit was purchased from Beyotime (Cat# C0117, Shanghai, China). The Nissl staining was applied according to previous work [24]. Sections were washed twice with ddH_2O and immersed in Nissl solution. Following dehydration and xylene clearing, the sections were sealed with neutral balsam. The images were acquired with an Olympus VS120 microscope (Tokyo, Japan). The area of cerebellar vermis and lobule thickness were measured by Olympus Oly VIA software.

Open Field Test

Mouse behavioral experiments were conducted in a quiet, clean environment. Each mouse was habituated to the behavioral testing room for 30 min before being placed in a 40 cm × 40 cm × 40 cm box. A mouse's unrestrained exploration was tracked by ANY-maze software (Stoelting, Illinois, USA) for 10 min.

Y-maze Test

The Y-maze consisted of three equal-length arms (30 cm × 6 cm × 15 cm). Each mouse was placed at the center of the maze and allowed to freely explore the three arms for 5 min. The standard for successful entry was when all four feet of the mouse were inside the arm. One alternation would be recorded if three arms were entered successively at a time. Spontaneous alternation (%) was calculated as: total alternations/(total arm entries − 2). Error (%) was calculated as: total errors/(total arm entries − 2).

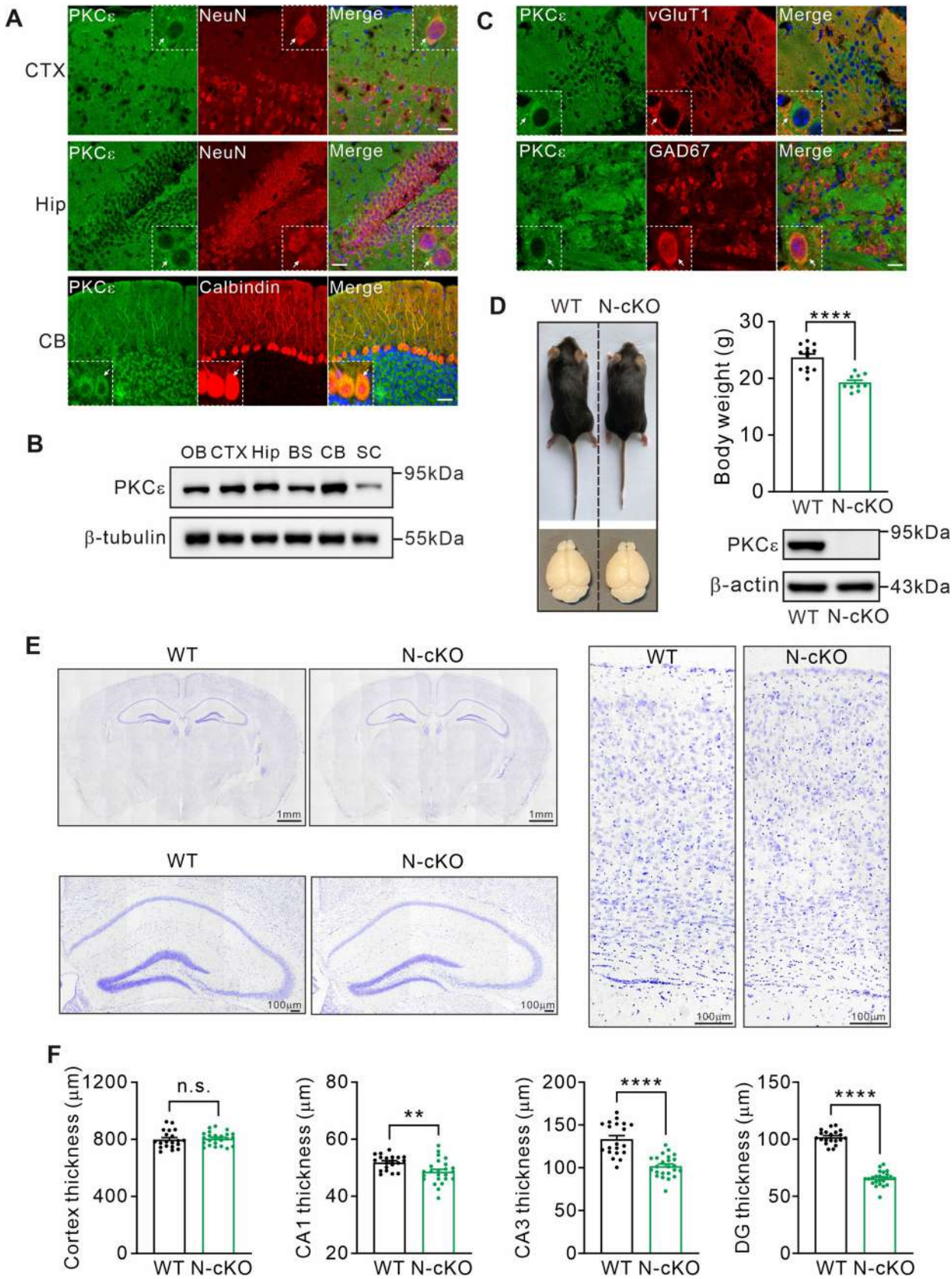
A
PKCε
NeuN
Merge
CTX
Hip
Calbindin
CB
C
vGluT1
GAD67
B
OB CTX Hip BS CB SC
95kDa
β-tubulin
55kDa
D
WT N-cKO
Body weight (g)
****
β-actin
43kDa
E
1mm
100μm
F
Cortex thickness (μm)
n.s.
CA1 thickness (μm)
**
CA3 thickness (μm)
DG thickness (μm)

◂**Fig. 1** PKCε deletion results in hippocampal atrophy. **A** Immunofluorescence staining of PKCε in the cerebral cortex (CTX), hippocampus (Hip), and cerebellum (CB). Cerebral cortex and hippocampus sections (2 months) are stained with PKCε and NeuN antibodies. Cerebellar sections (2 months) are stained with antibodies against PKCε and calbindin. The white arrows point to a Purkinje cell body. The experiment was performed 3 times. Scale bars, 50 μm. **B** Expression of PKCε in different mouse brain regions measured by immunoblotting. OB, olfactory bulbs; CTX, cerebral cortex; Hip, hippocampus; BS, brain stem; CB, cerebellum; SC, spinal cord. β-tubulin is the internal control. The experiment was performed 3 times. **C** Immunofluorescence staining of PKCε and vGluT1 or GAD67 in cerebral cortex. Scale bars, 50 μm. **D** N-cKO mice (2 months) display lower body weight. The knockout efficiency is confirmed by immunoblotting of PKCε in WT and N-cKO cerebellum (2 months). β-actin is the internal control. The experiment was performed 3 times. **E** Nissl staining in the cerebral cortex and hippocampus from WT and N-cKO mice (2 months). Scale bars, 1 mm (top left), 100 μm. **F** The thickness of the cerebral cortex and hippocampus CA1, CA3, and DG of WT and N-cKO mice. For statistics, see Supplementary Tables. $^{**}P < 0.01$, $^{****}P < 0.0001$.

Rotarod Test

After getting accustomed to rotation at a fixed speed of 5 r/min, each mouse was subjected to an accelerated rotation test. The trial was conducted twice a day, 8 h apart, for 4 days. The rotational speed was increased from 9 r/min to 50 r/min in 5 min.

Elevated Beam Test

Each mouse moved freely on a wooden beam (1 m in length, 1 cm in diameter, positioned 0.5 m above the ground). The slip percentage (%) was calculated as: number of slips of the hind paws/total number of steps.

Footprint Test

A white absorbent paper was placed on the floor of the Plexiglas tunnel (100 cm × 10 cm × 10 cm, length × width × height). Each mouse was allowed to freely traverse in the tunnel after a hindpaw was painted with non-toxic ink. Stride length and stance width were measured.

Three-Chamber Social Test

Three-chamber tests were applied as previously described [24]. The time spent in close interaction by the test mouse in each chamber was recorded as follows: t_E (time of close contact with the empty chamber), t_{S1} (time of close contact with the stranger 1 mouse), and t_{S2} (time of close contact with the stranger 2 mouse). The preference index for S1 over E (S1-E) was calculated as: $(t_{S1} - t_E)/(t_{S1} + t_E)$. The preference index for S2 over S1 (S2-S1) was calculated as: $(t_{S2} - t_{S1})/(t_{S2} + t_{S1})$.

Statistical Analysis

Data were analyzed using GraphPad Prism 9 (GraphPad Software, San Diego, USA) and Excel 2016 (Microsoft, Seattle, USA). The data analysis was independent of experimental conditions. Statistical differences were determined using a two-tailed unpaired Student's *t*-test or one-way analysis of variance (ANOVA). The accepted level of significance was $P < 0.05$. Data are presented as the mean ± SEM, *n* represents the number of animals used in behavioral tests or the number of experimental repetitions.

Results

PKCε Deletion Results in Hippocampal Atrophy

It has been shown that PKCε is expressed in the neonatal and adult brain [25]. Likewise, our results revealed that PKCε was expressed in multiple brain regions, including the cerebral cortex, hippocampus, and cerebellum (Fig. 1A, B). Moreover, PKCε co-localized with vesicular glutamate transporter 1 (vGluT1) or GAD67 (Fig. 1C), suggesting that PKCε is expressed in both excitatory and inhibitory neurons.

To investigate the functions of PKCε in the brain, $PKC\varepsilon^{F/F}$ mice were generated with the design of two LoxP sites adjacent to exon 2 of *Prkce* (Fig. S1A). Conditional knockout mice ($PKC\varepsilon^{F/F}$;$Nestin^{Cre}$; N-cKO) were generated by crossing $PKC\varepsilon^{F/F}$ (wild type, WT) with $Nestin^{Cre}$ mice. Ai9 reporter mice expressing tdTomato were crossed with $Nestin^{Cre}$ mice to ensure the expression of Cre-recombinase. Indeed, tdTomato fluorescence was found in the cerebellum, hippocampus, cerebral cortex, and other brain regions (Fig. S1B). There was no difference in the birth rate between N-cKO and WT mice; however, the body weight of N-cKO mice was slightly lower than WT mice (Fig. 1D). We next investigated whether PKCε deficiency affects the development of the cerebral cortex. Using Nissl staining in cerebral sections from WT and N-cKO mice, we found that the thickness of the cerebral cortex from N-cKO mice was grossly normal compared to WT mice. In contrast, there was a significant reduction in the thickness of the hippocampal CA1, CA3, and dentate gyrus (DG) areas (Fig. 1E, F).

PKCε Deletion Impairs Memory and Social Behaviors

With the advance of clinical diagnosis, intellectual disability has been clearly identified in SHORT syndrome [3–5]. Therefore, we examined PKCε cKO mice using several behavioral tests. The open-field test was first applied, and the N-cKO mice demonstrated normal time

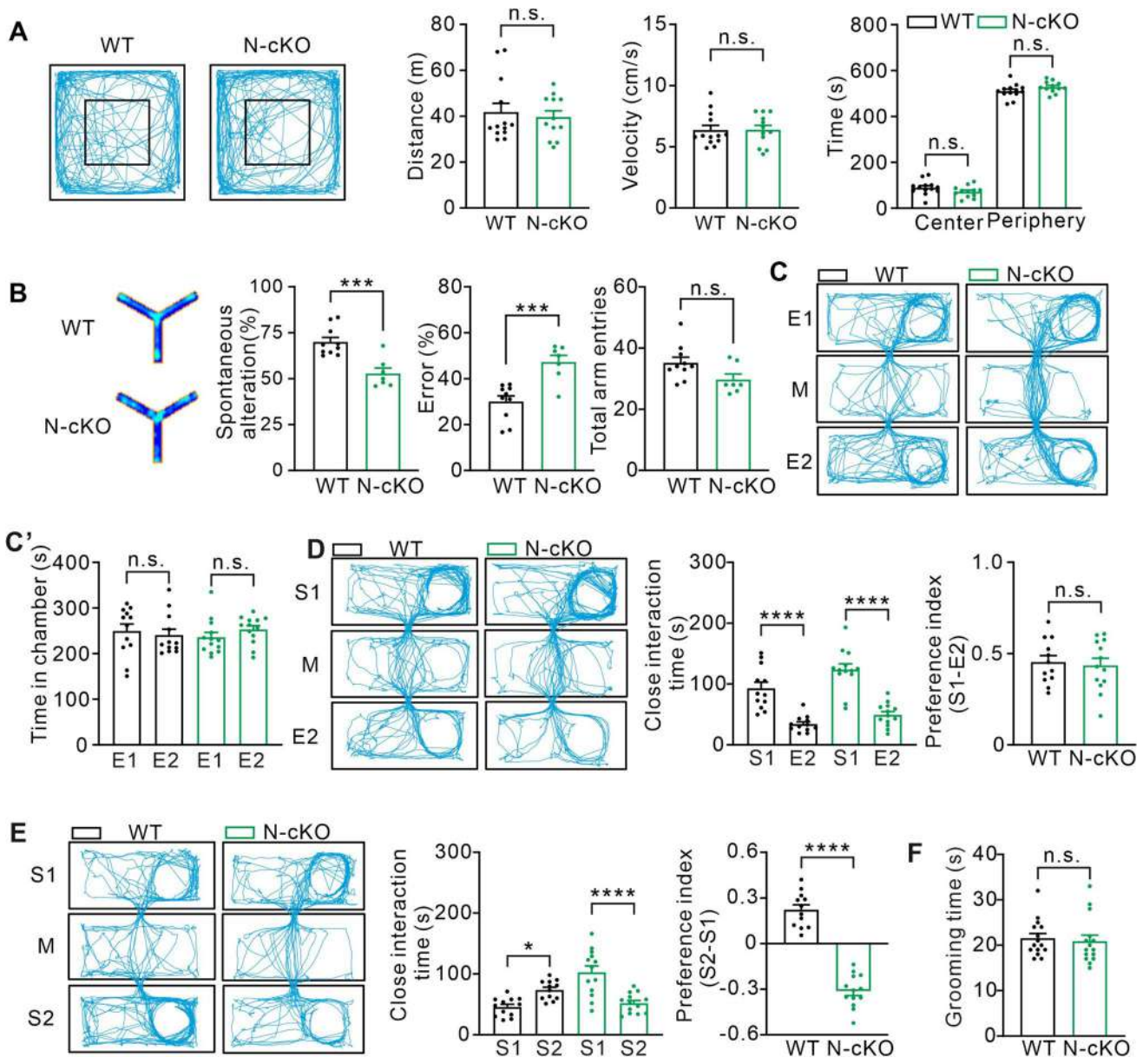

Fig. 2 PKCε deletion impairs working memory and social behaviors in male mice. **A** Open field test. WT (n = 13) and N-cKO mice (n = 12) show no differences in distance travelled, velocity, and time in the center or periphery. **B** N-cKO mice (n = 7) display normal alternation in the Y-maze test compared with WT (n = 10). **C** Example movement traces in the three-chamber test. **C'** The time spent in empty 1 (E1) and empty 2 (E2) by WT (n = 12) and N-cKO (n = 13) mice. **D** Example movement traces in the three-chamber test, close interaction time, and preference index (S1-E2) of WT (n = 12) and N-cKO (n = 13) mice. **E** Example movement traces in the three-chamber test, close interaction time, and preference index (S2-S1) of WT (n = 12) and N-cKO (n = 13) mice. **F** Self-grooming time of WT (n = 15) and N-cKO (n = 15) mice. For statistics, see the Supplementary Table. $^{**}P$ <0.01, $^{***}P$ <0.001, $^{****}P$ <0.0001.

in the center and peripheral zones compared to WT mice (Fig. 2A). However, during the Y-maze test, N-cKO mice showed significant impairment in spontaneous alternation compared to WT mice (Fig. 2B), indicating that N-cKO mice are deficient in short working memory. In the three-chamber test, neither WT nor N-cKO mice showed a preference for location during habituation (Fig. 2C). The N-cKO mice showed normal preferences during the sociability test (Fig. 2D), but had fewer close interactions with stranger 2 (S2) than stranger 1 (S1) mice during the social novelty test (Fig. 2E), indicating that PKCε deletion impairs social novelty. Besides,

N-cKO mice showed a normal grooming frequency in the self-grooming test compared to WT mice (Fig. 2F). Taken together, these results indicate that PKCε deletion affects memory and social behavior in male mice.

PKCε Deletion Impairs Cerebellar Development and Motor Coordination

Subsequently, we explored the involvement of PKCε in cerebellar development and motor functions. Nissl staining demonstrated that, compared to WT mice, there was a significant reduction in the total area of cerebellar cortex in N-cKO mice, and the thickness of the lobules was also decreased in N-cKO mice (Fig. 3A). Immunostaining for calbindin and NeuN indicated that the thickness of both the granule cell layer and the molecular layer was also reduced; meanwhile, the numbers of Purkinje cells (PCs) in all lobules were reduced in the N-cKO cerebellum (Fig. 3B).

Cerebellar atrophy has been reported to be associated with impaired synaptogenesis and reduced expression of synaptic proteins [26]. In light of this, we detected excitatory synaptic glutamate receptors, along with vesicular glutamate transporter 1 and 2 (vGluT1 and vGluT2), the synaptic markers for parallel fiber-PC and climbing fiber-PC synapses, respectively, in WT and N-cKO mice. Western blots demonstrated that deletion of PKCε significantly decreased the expression levels of ionotropic glutamate receptors (GluA1 and GluA2) and metabotropic glutamate receptors (mGlu1), as well as vGluT1 and vGluT2, in the cerebellum (Fig. 3C). These findings confirm that PKCε deficiency leads to defects in synaptic development.

Given that the neurological features of SHORT syndrome include impaired motor coordination [27, 28], we subsequently evaluated motor behaviors in N-cKO mice. The results demonstrated that N-cKO mice exhibited an abnormal gait: compared with control mice, their hind leg stride length was significantly reduced, and their stance width was markedly increased (Fig. 3D). To further examine the motor capabilities of N-cKO mice, we applied the elevated beam balance test and rotarod tests. The beam test revealed impaired balance in N-cKO mice (Fig. 3E), while the rotarod test indicated poor motor learning, as evidenced by minimal improvement across the test (Fig. 3F).

PKCε Deletion in GABAergic Neurons Does Not Induce Brain Atrophy

It has been reported that PKCε plays a crucial role in regulating the transport and activity of γ-aminobutyric acid A ($GABA_A$) receptors [29, 30], which are associated with several neurological disorders [31–33]. To determine whether PKCε deficiency affects the development of GABAergic neurons, we generated *PKCε*$^{F/F}$;*vGAT-Cre* (V-cKO) mice by crossing *PKCε*$^{F/F}$ mice with vesicular GABA transporter-Cre (*vGAT-Cre*) transgenic mice. Western blot and RT-PCR analyses provided evidence for the successful deletion of PKCε in neurons (Fig. S2A, B). V-cKO mice showed normal body weight and brain morphology (Fig. S2A). Nissl staining demonstrated that the thickness of the cerebral cortex in V-cKO mice was similar to that in control mice (Fig. 4A). There were no significant differences in the thickness of the CA1, CA3, and DG regions of the hippocampus (Fig. 4B). In addition, the area of the cerebellar vermis and the thickness of cerebellar lobules in V-cKO mice were within normal limits (Fig. 4C). Moreover, there were no significant changes in the thickness of the cerebellar granule layer and molecular layer, and the number of PCs across each lobule remained unchanged (Fig. 4D). Overall, these results suggest that knocking out PKCε in GABAergic neurons neither disrupts the development nor compromises the structural integrity of the cerebral cortex and cerebellum.

PKCε Deficiency Influences the Activation of AKT

Impaired activation of AKT *via* the PI3K-dependent pathway has been identified as a key contributing factor to SHORT syndrome [6–10]. To explore the potential connection between PKCε and AKT, we analyzed the expression levels of PKCε, AKT, and PI3K in the cerebellum during different developmental stages. Our results showed that PKCε and AKT displayed highly similar spatiotemporal expression patterns (Fig. 5A), suggesting a possible functional relationship between the two molecules. Subsequently, we used the Co-IP technique to evaluate the binding of PKCε to AKT. The results demonstrated that AKT was strongly detected in the PKCε immunoprecipitated fraction (Fig. 5B), providing evidence for the direct interaction between PKCε and AKT. Since the activity of AKT is closely related to the phosphorylation of the Thr308 and Ser473 residues [34], we measured the phosphorylation levels of AKT in the cerebellum of both control and N-cKO mice. Significantly, compared with controls, the expression of both AKT-pS473 and AKT-pT308 was markedly reduced in N-cKO mice (Fig. 5C).

In cultured N2A cells, treatment with the PKCε agonist DCP-LA (100 nmol/L) for 30 min significantly increased the phosphorylation levels of AKT at Thr308 and Ser473, while leaving total AKT expression unchanged (Fig. 5C, D). These results indicate that PKCε can enhance the activity of AKT.

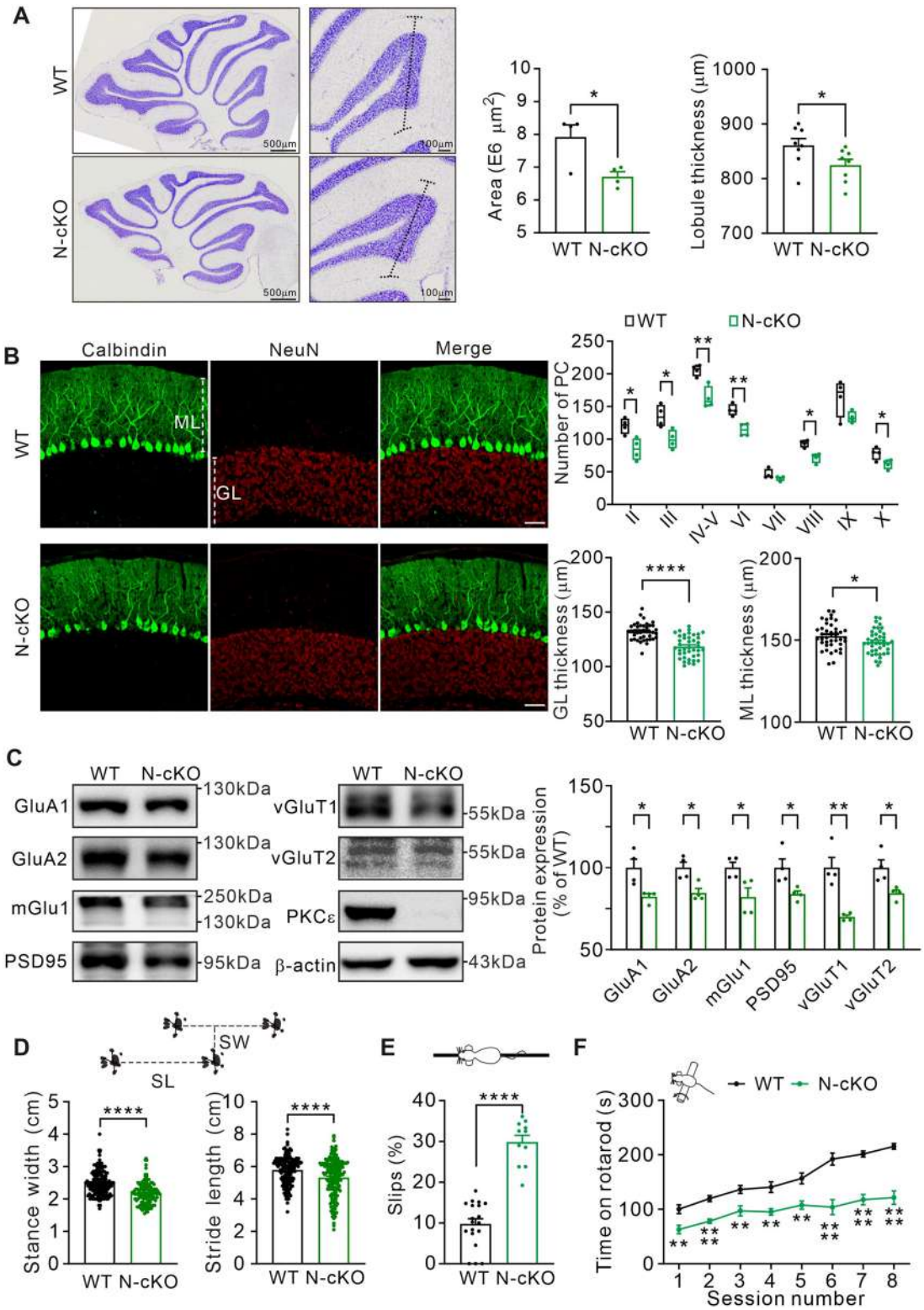

Moreover, stimulation with the PI3K agonist 740 Y-P (20 μmol/L, 30 min) induced a notable increase in the membrane translocation of PKCε in N2A cells (Fig. 5E, F), suggesting that PI3K regulates the subcellular localization of PKCε. In addition, VEGF-induced activation of PI3K led to an up-regulation of AKT phosphorylation at Ser473 and Thr308,

◂**Fig. 3** PKCε deletion leads to cerebellar atrophy and motor coordination disorders. **A** Nissl staining in the cerebellum from WT and N-cKO mice (2 months) showing the area of cerebellar vermis (left, scale bar, 500 μm) and the thickness of lobule III (right, scale bar, 100 μm). **B** Immunofluorescent staining in WT and N-cKO mice (2 months) showing the number of Purkinje cells, the thickness of the granule cell layer (GL), and the molecular layer (ML). $n = 4$ mice per group. Scale bar, 50 μm. **C** Immunoblots of protein expression of GluA1, GluA2, mGlu1, PSD95, vGluT1, vGluT2, and PKCε in WT and N-cKO cerebellum. β-actin is an internal control. $n = 6$ per group. **D** Footprints of the hindpaw of WT and N-cKO male mice showing stance width and stride length. **E** Percentage of steps involving hindpaw slips while walking on an elevated horizontal beam. **F** Time spent by WT and N-cKO male mice on the accelerating rotarod. For statistics, see the Supplementary Table. $^{*}P < 0.05$, $^{**}P < 0.01$, $^{****}P < 0.0001$.

which was effectively blocked by the PKCε translocation inhibitor εV1-2 (Fig. 5G). Overall, these findings suggest a model in which PI3K promotes the phosphorylation and translocation of PKCε, thereby facilitating the activation of AKT (Fig. 5H).

Discussion

PKCε has emerged as the second molecule associated with SHORT syndrome. However, additional evidence is required to firmly establish the link between PKCε and SHORT syndrome [14]. In this study, we investigated the functions of PKCε in regulating brain development and associated behaviors. Our data demonstrate that PKCε is intricately involved in PI3K-induced AKT activation, and plays a crucial role in regulating cerebellar development, motor coordination, and social behaviors. Overall, these findings suggest that PKCε could be a promising therapeutic target for treating SHORT syndrome. Notably, the PKCε agonist DCP-LA can enhance AKT activity.

Our work suggests a profound physiological and functional relationship between the PKCε and AKT pathways. First, both AKT and PKCε have been implicated in growth retardation. AKT deficiency leads to growth retardation in mice [35], and reduced AKT/mammalian target of rapamycin (mTOR) activity results in decreased protein synthesis [36]. Similarly, N-cKO mice exhibit reduced body size and cerebellar atrophy (Figs 1D, 3A). Second, both AKT and PKCε are associated with cognitive disorders. AKT/glycogen synthase kinase 3β (GSK3β), AKT/mTOR, and AKT/FoxO1 signaling pathways are linked to Alzheimer's disease (AD) through regulating β-amyloid and phospho-tau aggregates; meanwhile, restoring AKT activity can rescue the cognitive impairment in AD [37–39]. Likewise, the activation of PKCε also ameliorates cognitive impairment, and reduced expression of PKCε has been reported in the hippocampal neurons of AD patients, accompanied by elevated levels of Aβ [18, 20]. Bryostatin-1 improves cognitive functions in AD patients by activating PKCε [19]. In the present work, we found that N-cKO mice display deficits in working memory and social novelty recognition. Third, the AKT and PKCε pathways are associated with motor disorders. AKT activity is reduced in the substantia nigra pars compacta of Parkinson's disease patients [40]. Similarly, N-cKO mice exhibited motor coordination disorders. Given that PKCε deficiency down-regulates AKT activity in N-cKO mice, the motor and cognitive impairments caused by PKCε deficiency may be attributed to the altered AKT activity. Moreover, the down-regulation of AKT activity may be the primary cause of brain atrophy and cognitive impairment in patients with PKCε-relevant SHORT syndrome.

The present study provides compelling evidence demonstrating that PKCε mutations are responsible for SHORT syndrome. The hallmark features of SHORT syndrome include growth retardation and insulin resistance [2, 14]. Consistent with this, PKCε-deficient mice exhibit reduced body size. Furthermore, it has been reported that PKCε modulates the activity of insulin receptors and induces hepatic insulin resistance through Thr1160 phosphorylation [41]. The patients with SHORT syndrome display motor impairments; meanwhile, abnormal gait, motor imbalance, and reduced motor learning were observed in PKCε-deficient mice as well. Microcephaly and intellectual disability have been documented in patients with SHORT syndrome [3–5], which aligns with the hippocampal and cerebellar atrophy and cognitive deficits discovered in PKCε-deficient mice.

There are some caveats in the present study: (i) It has been reported that a heterozygous mutation in PKCε (E599K) is associated with SHORT syndrome; this reduces the activity of PKCε without altering its expression [14]. Here, we applied the Cre-loxP strategy to delete the second exon of *Prkce*, resulting in a frame-shift mutation. This approach differs from the E599K mutation, which may induce more severe developmental or behavioral phenotypes; (ii) PKCε is implicated in the functional regulation of GABA receptors [29, 30]. However, the architecture of the hippocampus and cerebellum was intact in V-cKO mice, where PKCε was deleted in GABAergic neurons. We hypothesize that PKCε may function across different neuronal populations and the deficiency of PKCε in glutamatergic neurons or glial cells may decisively lead to brain atrophy [42, 43]; and (iii) We found that PKCε deficiency has little impact on the cortical thickness. This may be related to the lower activity of AKT in the cortical area. To address this question, we examined the phosphorylation levels of AKT in the cortex, hippocampus, and cerebellum. Our results indicated that AKT-S473 phosphorylation in the cortex was the lowest compared to that in the hippocampus or cerebellum (Fig. S3A), which

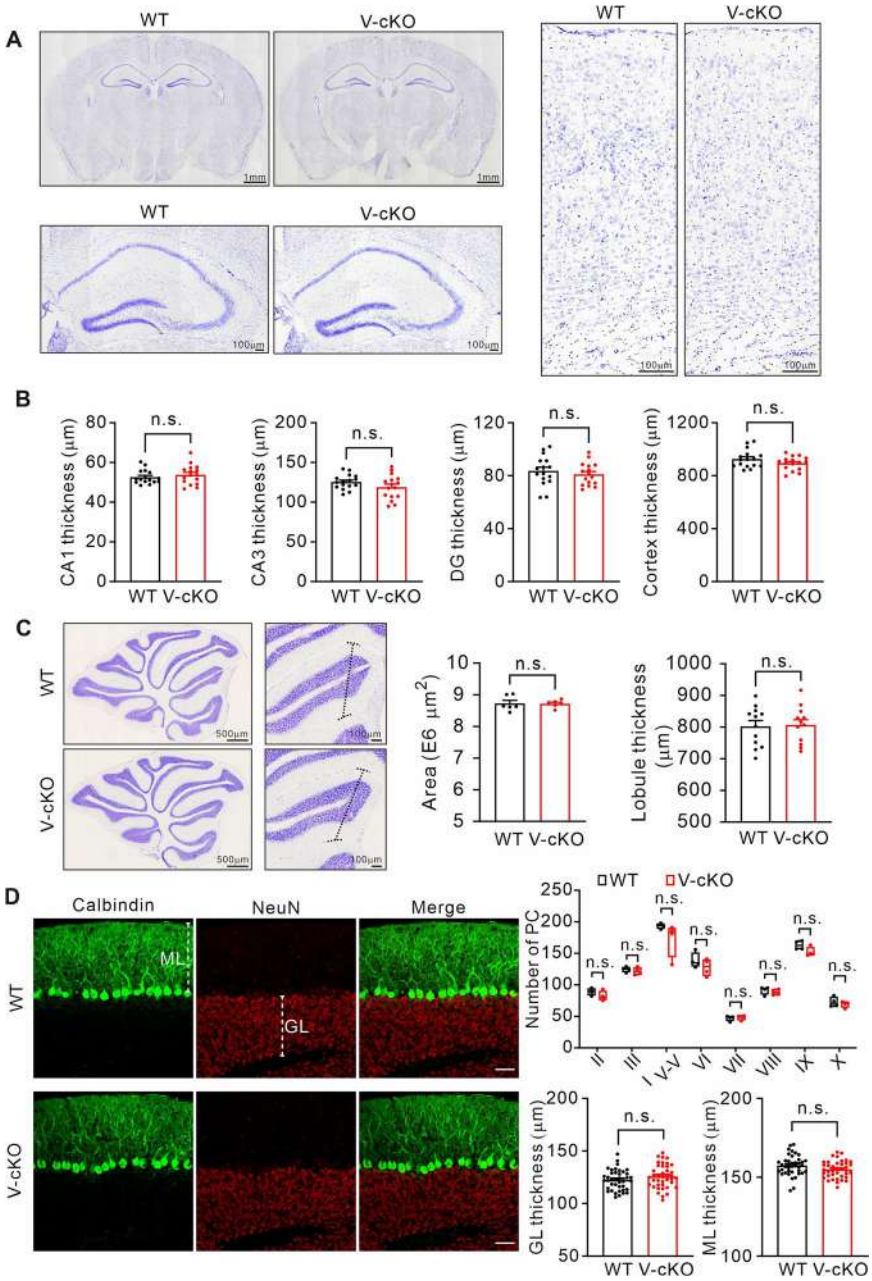

Fig. 4 Cerebral and cerebellar cyto-architecture is normal in V-cKO mice. **A** Nissl staining in the cerebral cortex and hippocampus from WT and V-cKO mice (2 months). Scale bars, 1 mm (top left), 100 μm. **B** The thickness of the cerebral cortex and hippocampal CA1, CA3, and DG of WT and N-cKO mice. **C** Nissl staining in the cerebellum from WT and V-cKO mice (2 months) showing the area of cerebellar vermis (left, scale bar, 500 μm) and the thickness of lobule III (right, scale bar, 100 μm). **D** Immunofluorescent staining of WT and V-cKO cerebellum sections with calbindin and NeuN antibodies and the number of Purkinje cells (PCs), the thickness of the granule cell layer (GL), and the molecular layer (ML). $n = 4$ mice per group. Scale bars, 50 μm. For statistics, see the Supplementary Table. n.s. $P > 0.05$.

may explain the minimal impact of PKCε deficiency on cortical development.

In summary, the present study, for the first time, systematically investigated the pathological consequences of PKCε deficiency in the central nervous system using multiple conditional knockout mouse models. We found that PKCε mediates the VEGF/PI3K-mediated activation of AKT, thereby impacting hippocampal and cerebellar atrophy and cognitive behaviors in mice. This study offers novel insights into the neurological manifestations associated with SHORT syndrome.

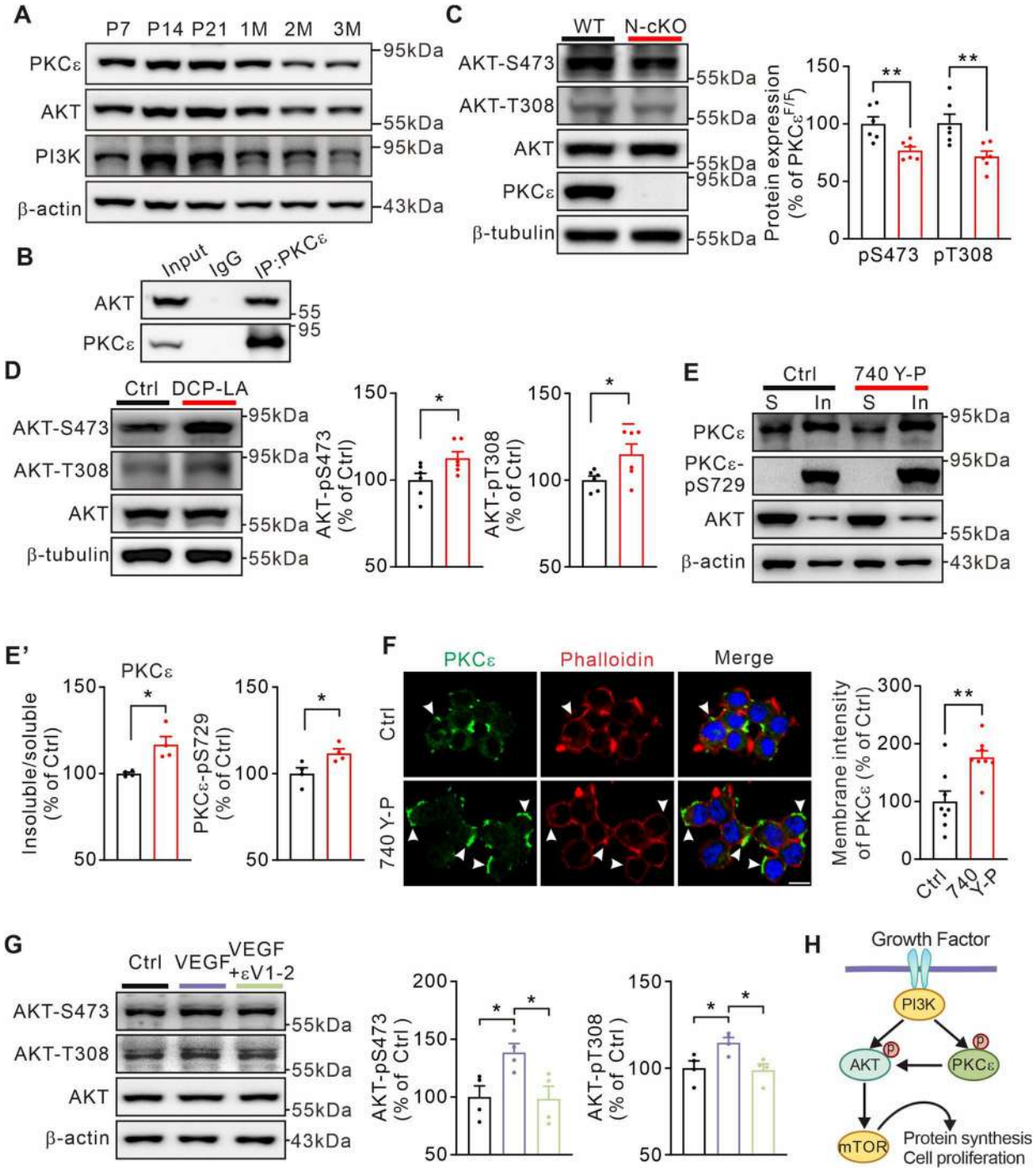

Fig. 5 PKCε is involved in PI3K-induced AKT activation. **A** Expression of PKCε, AKT, and PI3K in the mouse cerebellum of different ages. P7, postnatal day 7; 1M, postnatal 1 month. β-actin is the internal control. The experiment was performed 3 times. **B** Total cerebellar lysates are immunoprecipitated with rabbit anti-PKCε antibody, and immunoprecipitates are probed with antibodies to PKCε and AKT. Rabbit IgG is used as the negative control. The experiment was performed 3 times. **C** The phosphorylation of AKT (AKT-S473, AKT-T308) in WT and N-cKO cerebellum tested by immunoblotting. AKT is an internal control. $n = 6$ per group. **D** The phosphorylation of AKT (AKT-S473, AKT-T308) tested after DCP-LA treatment for 60 min in N2A cells. $n = 6$. **E** Expression of PKCε in Triton X-insoluble (In) and soluble (S) fractions of N2A cells after 740 Y-P treatment for 60 min. The histogram shows the ratios of Triton X-insoluble (In)/ soluble (S) fraction. $n = 4$. **F** N2A cells treated with 740 Y-P for 60 min. Immunofluorescent staining of PKCε with phalloidin (F-actin)-labeled cell membrane. White arrowheads show the membrane-associated PKCε. Scale bar, 10 μm. The experiment was performed 3 times. **G** The phosphorylation of AKT (AKT-S473, AKT-T308) tested after VEGF or VEGF + εV1-2 treatment for 60 min in N2A cells. $n = 4$. For statistics, see the Supplementary Table. $^*P < 0.05$, $^{**}P < 0.01$.

Acknowledgements This work was supported by Zhejiang Province Natural Science Foundation (LMS25C090003), the National Natural Science Foundation of China (32200816 and 32000692), and Autism Research Special Fund of Zhejiang Foundation for Disabled Persons (2024003).

Data Availability All relevant data supporting the present study are uploaded as supporting information for online publication.

Conflict of interest The authors declare that they have no competing interests.

References

1. Innes AM, Dyment DA, SHORT Syndrome. GeneReviews 2020, 1993–2025
2. Avila M, Dyment DA, Sagen JV, St-Onge J, Moog U, Chung BY. Clinical reappraisal of SHORT syndrome with PIK3R1 mutations: toward recommendation for molecular testing and management. Clin Genet 2016, 89: 501–506.
3. Zhang Y, Ji B, Li J, Li Y, Zhang M, Ban B. SHORT syndrome in two Chinese girls: A case report and review of the literature. Mol Genet Genomic Med 2020, 8: e1385.
4. Patel V, Cui W, Cobben JM. SHORT syndrome with microcephaly and developmental delay. Am J Med Genet A 2023, 191: 850–854.
5. Gonçalves ACG, Moretti PN, Cordoba MS, Oliveira RS, Lopes FSC, Oliveira SF, *et al*. SHORT syndrome in an adult Brazilian patient. Am J Med Genet A 2022, 188: 1635–1638.
6. Huang-Doran I, Tomlinson P, Payne F, Gast A, Sleigh A, Bottomley W, *et al*. Insulin resistance uncoupled from dyslipidemia due to C-terminal PIK3R1 mutations. JCI Insight 2016, 1: e88766.
7. Winnay JN, Solheim MH, Dirice E, Sakaguchi M, Noh HL, Kang HJ, *et al*. PI_3^-kinase mutation linked to insulin and growth factor resistance *in vivo*. J Clin Invest 2016, 126: 1401–1412.
8. Solheim MH, Clermont AC, Winnay JN, Hallstensen E, Molven A, Njølstad PR, *et al*. Iris malformation and anterior segment dysgenesis in mice and humans with a mutation in PI 3-kinase. Invest Ophthalmol Vis Sci 2017, 58: 3100–3106.
9. Solheim MH, Winnay JN, Batista TM, Molven A, Njølstad PR, Ronald Kahn C. Mice carrying a dominant-negative human PI3K mutation are protected from obesity and hepatic steatosis but not diabetes. Diabetes 2018, 67: 1297–1309.
10. Kwok A, Zvetkova I, Virtue S, Luijten I, Huang-Doran I, Tomlinson P, *et al*. Truncation of Pik3r1 causes severe insulin resistance uncoupled from obesity and dyslipidaemia by increased energy expenditure. Mol Metab 2020, 40: 101020.
11. Tsay A, Wang JC. The role of PIK3R1 in metabolic function and insulin sensitivity. Int J Mol Sci 2023, 24: 12665.
12. Yu JSL, Cui W. Proliferation, survival and metabolism: the role of PI3K/AKT/mTOR signalling in pluripotency and cell fate determination. Development 2016, 143: 3050–3060.
13. He X, Li Y, Deng B, Lin A, Zhang G, Ma M, *et al*. The PI3K/AKT signalling pathway in inflammation, cell death and glial scar formation after traumatic spinal cord injury: mechanisms and therapeutic opportunities. Cell Prolif 2022, 55: e13275.
14. Alcantara D, Elmslie F, Tetreault M, Bareke E, Hartley T, Consortium C, et al. SHORT syndrome due to a novel *de novo* mutation in PRKCE (Protein Kinase Cε) impairing TORC2-dependent AKT activation. Hum Mol Genet (2017), 26: 3713–3721
15. Kawano T, Inokuchi J, Eto M, Murata M, Kang JH. Protein kinase C (PKC) isozymes as diagnostic and prognostic biomarkers and therapeutic targets for cancer. Cancers (Basel) 2022, 14: 5425.
16. Kumashiro N, Erion DM, Zhang D, Kahn M, Beddow SA, Chu X, *et al*. Cellular mechanism of insulin resistance in nonalcoholic fatty liver disease. Proc Natl Acad Sci U S A 2011, 108: 16381–16385.
17. Zheng ZG, Xu YY, Liu WP, Zhang Y, Zhang C, Liu HL, *et al*. Discovery of a potent allosteric activator of DGKQ that ameliorates obesity-induced insulin resistance *via* the Sn-1, 2-DAG-PKCε signaling axis. Cell Metab 2023, 35: 101-117.e11.
18. Khan TK, Sen A, Hongpaisan J, Lim CS, Nelson TJ, Alkon DL. PKCε deficits in Alzheimer's disease brains and skin fibroblasts. J Alzheimers Dis 2015, 43: 491–509.
19. Nelson TJ, Sun MK, Lim C, Sen A, Khan T, Chirila FV, *et al*. Bryostatin effects on cognitive function and PKCε in Alzheimer's disease phase IIa and expanded access trials. J Alzheimers Dis 2017, 58: 521–535.
20. Sen A, Nelson TJ, Alkon DL, Hongpaisan J. Loss in PKC *Epsilon* causes downregulation of MnSOD and BDNF expression in neurons of Alzheimer's disease hippocampus. J Alzheimers Dis 2018, 63: 1173–1189.
21. Chen L, Wang H, Xing J, Shi X, Huang H, Huang J, *et al*. Silencing P2X7R alleviates diabetic neuropathic pain involving TRPV1 *via* PKCε/P38MAPK/NF-κB signaling pathway in rats. Int J Mol Sci 2022, 23: 14141.
22. Hanim A, Mohamed IN, Mohamed RMP, Mokhtar MH, Makpol S, Naomi R, *et al*. Alcohol dependence modulates amygdalar mTORC2 and PKCε expression in a rodent model. Nutrients 2023, 15: 3036.
23. Wang XT, Zhou L, Dong BB, Xu FX, Wang DJ, Shen EW, *et al*. cAMP-EPAC-PKCε-RIM1α signaling regulates presynaptic long-term potentiation and motor learning. Elife 2023, 12: e80875.
24. Zheng R, Xu FX, Zhou L, Xu J, Shen Y, Hao K, *et al*. Ablation of KIF2C in Purkinje cells impairs metabotropic glutamate receptor trafficking and motor coordination in male mice. J Physiol 2023, 601: 3905–3920.
25. Schaffer TB, Smith JE, Cook EK, Phan T, Margolis SS. PKCε inhibits neuronal dendritic spine development through dual phosphorylation of Ephexin5. Cell Rep 2018, 25: 2470-2483.e8.
26. Yang Y, Huang G, Jiang X, Li X, Sun K, Shi Y, *et al*. Loss of Wtap results in cerebellar ataxia and degeneration of Purkinje cells. J Genet Genom 2022, 49: 847–858.
27. Bravo García-Morato M, García-Miñaúr S, Molina Garicano J, Santos Simarro F, Del Pino Molina L, López-Granados E, *et al*. Mutations in PIK3R1 can lead to APDS2, SHORT syndrome or a combination of the two. Clin Immunol 2017, 179: 77–80.
28. Szczawińska-Popłonyk A, Bernat-Sitarz K, Schwartzmann E, Piechota M, Badura-Stronka M. Clinical and immunological assessment of APDS2 with features of the SHORT syndrome related to a novel mutation in *PIK3R1* with reduced penetrance. Allergol Immunopathol (Madr) 2022, 50: 1–9.
29. Hodge CW, Raber J, McMahon T, Walter H, Sanchez-Perez AM, Olive MF, *et al*. Decreased anxiety-like behavior, reduced stress hormones, and neurosteroid supersensitivity in mice lacking protein kinase Cepsilon. J Clin Invest 2002, 110: 1003–1010.
30. Qi ZH, Song M, Wallace MJ, Wang D, Newton PM, McMahon T, *et al*. Protein kinase C epsilon regulates gamma-aminobutyrate type A receptor sensitivity to ethanol and benzodiazepines through phosphorylation of gamma2 subunits. J Biol Chem 2007, 282: 33052–33063.
31. Marín O. Interneuron dysfunction in psychiatric disorders. Nat Rev Neurosci 2012, 13: 107–120.
32. Shi Y, Wang M, Mi D, Lu T, Wang B, Dong H, *et al*. Mouse and human share conserved transcriptional programs for interneuron development. Science 2021, 374: eabj6641.
33. Pilotto F, Douthwaite C, Diab R, Ye X, Al Qassab Z, Tietje C, *et al*. Early molecular layer interneuron hyperactivity triggers Purkinje neuron degeneration in SCA1. Neuron 2023, 111: 2523-2543.e10.

34. Guo N, Wang X, Xu M, Bai J, Yu H, Zhang L. PI3K/AKT signaling pathway: molecular mechanisms and therapeutic potential in depression. Pharmacol Res 2024, 206: 107300.
35. Chen WS, Xu PZ, Gottlob K, Chen ML, Sokol K, Shiyanova T, *et al*. Growth retardation and increased apoptosis in mice with homozygous disruption of the Akt1 gene. Genes Dev 2001, 15: 2203–2208.
36. Chen Z, Li L, Wu W, Liu Z, Huang Y, Yang L, *et al*. Exercise protects proliferative muscle satellite cells against exhaustion *via* the Igfbp7-Akt-mTOR axis. Theranostics 2020, 10: 6448–6466.
37. Zhang W, Bai S, Yang J, Zhang Y, Liu Y, Nie J, *et al*. FoxO1 overexpression reduces Aβ production and tau phosphorylation *in vitro*. Neurosci Lett 2020, 738: 135322.
38. Querfurth H, Lee HK. Mammalian/mechanistic target of rapamycin (mTOR) complexes in neurodegeneration. Mol Neurodegener 2021, 16: 44.
39. Long HZ, Cheng Y, Zhou ZW, Luo HY, Wen DD, Gao LC. PI3K/AKT signal pathway: a target of natural products in the prevention and treatment of Alzheimer's disease and Parkinson's disease. Front Pharmacol 2021, 12: 648636.
40. Luo S, Kang SS, Wang ZH, Liu X, Day JX, Wu Z, *et al*. Akt phosphorylates NQO1 and triggers its degradation, abolishing its antioxidative activities in Parkinson's disease. J Neurosci 2019, 39: 7291–7305.
41. Petersen MC, Madiraju AK, Gassaway BM, Marcel M, Nasiri AR, Butrico G, *et al*. Insulin receptor Thr1160 phosphorylation mediates lipid-induced hepatic insulin resistance. J Clin Invest 2016, 126: 4361–4371.
42. Rubio-Casillas A, Fernández-Guasti A. The dose makes the poison: from glutamate-mediated neurogenesis to neuronal atrophy and depression. Rev Neurosci 2016, 27: 599–622.
43. He C, Duan S. Novel insight into glial biology and diseases. Neurosci Bull 2023, 39: 365–367.